Compact Super Wideband Optical Antenna

Wen C. Wang*, Richard Forber, and Kenneth Bui[a]
IPITEK, 2330 Faraday Ave., Carlsbad, CA 92008.
[a]U.S. Army CECOM, Fort Monmouth, NJ 07703

ABSTRACT

We present progress on advanced optical antennas, which are compact, small size-weight-power units capable to receive super wideband radiated RF signals from 30 MHz to over 3 GHz. Based on electro-optical modulation of fiber-coupled guided wave light, these dielectric E-field sensors exhibit dipole-like azimuthal omni directionality, and combine small size ($<< \lambda_{RF}$) with uniform field sensitivity over wide RF received signal bandwidth. The challenge of high sensitivity is addressed by combining high dynamic range photonic link techniques, multiple parallel sensor channels, and high EO sensing materials. The antenna system photonic link consists of a 1550 nm PM fiber-pigtailed laser, a specialized optical modulator antenna in channel waveguide format, a wideband photoreceiver, and optical phase stabilizing components. The optical modulator antenna design employs a dielectric (no electrode) Mach-Zehnder interferometer (MZI) arranged so that sensing RF bandwidth is not limited by optical transit time effects, and MZI phase drift is bias stabilized. For a prototype optical antenna system that is < 100 in^3, < 10 W, < 5 lbs, we present test data on sensitivity (< 20 $mV/m\text{-}Hz^{1/2}$), RF bandwidth, and antenna directionality, and show good agreement with theoretical predictions.

Keywords: Optical E-field sensors, optical receive antenna, MZI devices, EO material.

1. INTRODUCTION

Electric field sensors are being developed for use as a super wideband RF antenna, to meet needs for compact, small size-weight-power units capable to receive radiated RF signals from MHz to multiple GHz. In a previous work, we reported on the development of optical E-field sensors for wideband antenna application.[1,2] That work showed the basic advantages of using optical antennas, and compared theory and experiment for early versions of sensors based on LD3 polymer in Mach Zehnder Interferometer (MZI) optical sensor configuration. Optical antennas have several potential advantages over conventional copper-based RF antennas: small size, wide dynamic range, signal transport over non distorting and low loss optical fiber, wide bandwidth from MHz to 10's of GHz, good sensitivity (~few $mV/(m\sqrt{Hz})$), immunity to high (antenna-damaging) electric field strength, and they are minimally perturbing to surrounding antennas and electronics. Besides the wideband antenna use, there are many other broad applications including High Power Microwave (HPM) test and evaluation,[3] EMI testing and experimentation, hyperthermia treatment,[4] electromagnetic railgun test and evaluation, radio and radar receivers, electrically isolated antenna relay and remoting, and various array applications for spatial characterization or field propagation directionality.

Polymer MZI antenna devices we presented before offer a number of advantages to exploit for this antenna need: easy processing into antennas of different size and shape, the antenna elements can be easily configured and applied to different surfaces, sections of the polymer optical waveguides can separately be electrically poled to maximum benefit, device designs can be enhanced in the future based on continued advances in electro optic (EO) polymer materials as they become available. Much work continues on the development of new polymer materials that exhibit large EO coefficients, and these new materials can eventually address a wide variety of applications.[5,6]

* wwang@ipitek.com; phone 1 760 438-1010 x 3291; fax 1 760 438-2412; www.ipitek.com

Fiber Optic Sensors and Applications VI, edited by Eric Udd, Henry H. Du, Anbo Wang, Proc. of SPIE Vol. 7316, 731614
© 2009 SPIE · CCC code: 0277-786X/09/$18 · doi: 10.1117/12.818139

In our previous optical antennas work the polymer EO coefficient of LD3 was a limitation, being only about 8 pm/V. This is much smaller than that of the best new polymers and is also well below the capability of $LiNbO_3$ based devices. The limited availability and developing process ability of the new polymers keeps them from yet finding broad use. To move forward with our optical antenna development we currently leverage the benefits of $LiNbO_3$. It has high refractive index (2.2), moderate EO coefficient (30 pm/V), low optical transmission loss (< 0.2 dB/cm), and exhibits fiber-fiber insertion loss under 3 dB for long devices. Therefore, an optical antenna using $LiNbO_3$ will far exceed the performance we obtained in our prior work with LD3 polymer, and is our focus in this report.

We describe here the development of an all-dielectric $LiNbO_3$ field sensor antenna that employs a dielectric (no electrode) Mach-Zehnder interferometer (MZI) consists of two push-pull driven optical channel waveguides. It was arranged so that sensing RF bandwidth is not limited by optical transit time effects, and MZI phase drift is bias stabilized. These dielectric E-field sensors exhibit dipole-like azimuthal omni directionality, and combine small size ($\ll \lambda_{RF}$) with uniform field sensitivity over wide RF received signal bandwidth. The antenna system photonic link consists of a 1550 nm PM fiber-pigtailed laser, a specialized optical modulator antenna in channel waveguide format, a wideband photo detector, and optical phase stabilizing components.

2. FIELD SENSOR OPERATION THEORY

In the basic configuration of an MZI optical modulator, the EO active arms of the interferometer are oppositely poled (see Fig. 1b), in push-pull fashion. An external electric field applied uniformly to the push-pull arms causes a relative phase difference by the EO effect operating on the optical waves in the two arms, resulting in modulation of the MZI optical output intensity.

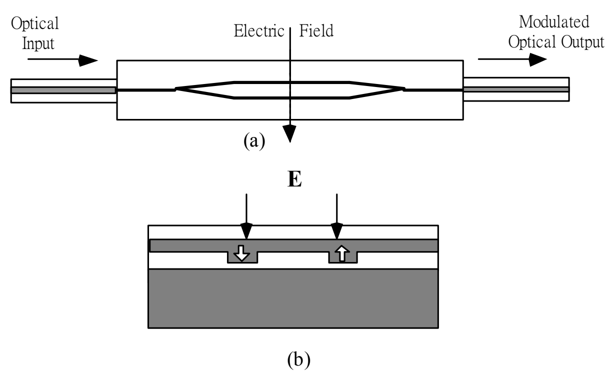

Fig. 1. A schematic design of the all-dielectric waveguide E-field sensor with push-pull configuration. When the sensor is subjected to an oscillating external field, an equal and opposite phase is built up between the MZI arms, leading to intensity modulation at the MZI output.

The output optical signal power at optimum MZI phase bias (quadrature) is modulated by an RF wave with electric field of E and frequency of Ω

$$P_o(\Omega_{RF})|_{mod} \sim P_L T_{IO} [E(\Omega_{RF})/E_\pi] \tag{1}$$

where T_{IO} is the input-to-output transmission factor due to insertion loss, P_L is the input optical power, and E_π is the electric field that would produce a full-on to full-off signal change. E_π depends on EO parameters as follows:

$$E_\pi = \lambda / (n^3 r_{eff} L), \tag{2}$$

where n is the index of refraction, r_{eff} is the effective EO coefficient, L is the length of the EO region optical path, and λ is the optical wavelength. From these simple dependencies it is clear that the output signal is improved by high optical power to the sensor, high optical transmission (low loss), and low E_π. As discussed below, $LiNbO_3$ has a much lower E_π than available polymers at this time, and it also handles high optical power (100's mW) with minimal insertion loss (~3 dB), as well.

2.1 Frequency Response Limitation

For use in photonic link applications, MZI modulators have been produced with frequency response of more than 40 GHz using $LiNbO_3$, and even 100 GHz using polymer EO materials which enable close phase matching between RF and optical fields.[7] However, for this all-dielectric optical antenna the frequency response is limited by the optical transit time of probe light through the active EO zone during the sensed RF field oscillation cycle. Depending on the RF field propagation direction with respect to the optical beam direction in the channel waveguides, the transit time and thus the frequency response will be different when this transit time is close to the RF cycle period. In the following we will first analyze the response of an EO MZI waveguide that is aligned normal to the propagating RF wavevector. The discussion of the other orientations will follow.

According to the analysis of Yariv[8] a phase change induced by electric field E on an EO material with EO coefficient r_{33} and length L is

$$\Gamma = \frac{2\pi n^3 r_{33}}{\lambda} EL = a_{EO} EL \tag{3}$$

First let's assume RF field propagates normal to EO waveguide. If the field E changes appreciably during the transit time, τ_d, of the light through the EO material:

$$\tau_d = \frac{nL}{c} \tag{4}$$

Eq (3) must be replaced by:

$$\Gamma(t) = a_{EO} \int_0^L E(t_p) dz = a_{EO} \int_{t-\tau_d}^{t} E(t_p) \frac{c}{n} dt_p \tag{5}$$

where c is the speed of light in vacuum, and $E(t)$ is the instantaneous RF electric field. In the second integral, at the right side of Eq. (5), we replaced integration over z by integration over time, t, recognizing that the portion of the wave that reaches the output of the EO material z = L at time t, entered the material at time $[\tau_d - t]$. We also assume that at any given moment the field $E(t)$ has the same value throughout the material.

Taking $E(t)$ as a sinusoid field, we obtain:

$$\Gamma(t) = a_{EO} \frac{c}{n} \int_{t-\tau_d}^{t} E \sin(\omega t_p) dt_p = a_{EO} \frac{c}{n} E \int_{t-\tau_d}^{t} \sin(\omega t_p) dt_p \tag{6}$$

Here ω is the RF frequency. Upon integration of the sinusoid term, one obtains:

$$\int_{t-\tau_d}^{t} \sin(\omega t_p) dt_p = \frac{1}{\omega}[\cos[\omega(t-\tau_d)] - \cos(\omega t)] = \frac{2}{\omega}[\sin[\omega(t - \frac{\tau_d}{2})]\sin(\frac{\omega \tau_d}{2})] \tag{7}$$

and thus:

$$\Gamma(t) = a_{EO} \frac{c}{n} E \frac{2}{\omega}[\sin[\omega(t - \frac{\tau_d}{2})]\sin(\frac{\omega \tau_d}{2})] \tag{8}$$

By rearranging Eq. (8) one obtains a concise and useful expression for the RF induced phase change:

$$\Gamma(t) = a_{EO} EL \frac{\sin(\frac{\omega\tau_d}{2})}{(\frac{\omega\tau_d}{2})} \sin[\omega(t - \frac{\tau_d}{2})] \tag{9}$$

Note that at time t, the optical probe is leaving the O-E active section.

According to Eq. (9), the RF accumulated retardation is oscillating at the RF frequency. Its amplitude is identical to the one obtained with DC fields, Eq. (3), multiplied by a reduction *sinc function* of $[\omega\tau_d/2]$. Therefore, the accumulated RF phase is a linear measure of the E-field, and only when $[\omega\tau_d] << 1$, maximum accumulated phase is expected. That means that the phase is linear with the EO active length, up to about 1/4 of the RF wavelength, λ_{rf}.

For RF wave propagating at an angle to the waveguide, the simplest geometry to analyze in this case is when the RF wave vector is collinear with the sensor waveguide. This is the *traveling wave case* that is generally used in high-speed modulators. If the RF and the optical wave are propagating with the same phase velocity, their interaction is maximized, and vice versa for counter propagating. The first case is called *phase matched traveling wave* where the sensor experiences no frequency limitation independent of its length.

In a general collinear case, the expression for the frequency dependence of the accumulated phase change, Eq. (9), is modified. The transit time is replaced by an effective shorter transit time term:

$$\tau_{para} = \tau_d (1 - \frac{n_{rf}}{n}) \tag{10}$$

While the case of counter-parallel propagation corresponds to an effective longer transit time term:

$$\tau_{count} = \tau_d (1 + \frac{n_{rf}}{n}) \tag{11}$$

Here n_{rf} is about 1 for RF wave propagating in the air. Note that for a push-pull MZI device, the accumulated phase change $\Gamma(t)$ should be double. Since the modulated optical intensity (Eq. 1) is proportional to Γ, the RF signal detected is proportional to Γ^2. For a 2 cm long EO polymer MZI device with refractive index of 1.6, the simulation results of frequency responses of RF signal with RF wave vector parallel, perpendicular, and counter-parallel to the waveguide, respectively, are shown in Fig. 2. For RF propagates at intermediate angles, the frequency response should fall in between those three curves.

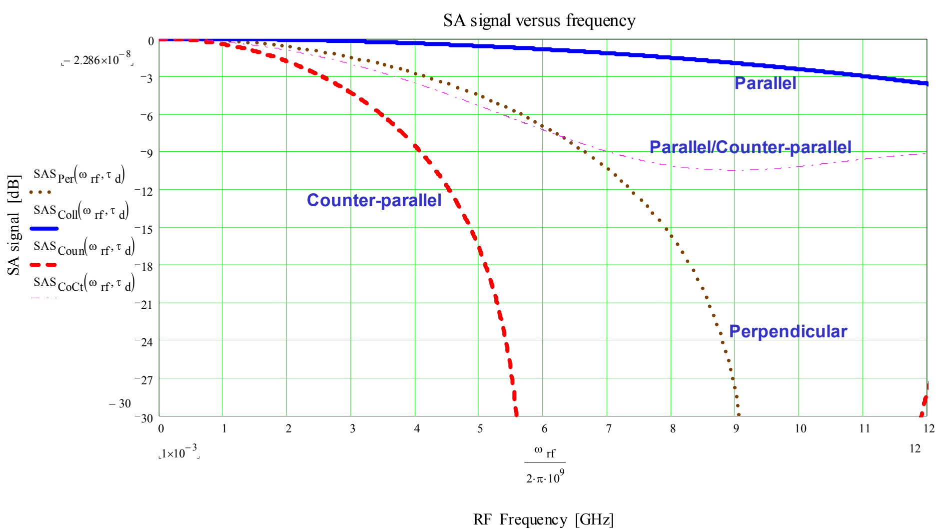

Fig. 2. . Simulation of the RF frequency response of a 20 mm EO polymer field sensor.

The key element for the frequency response behavior is the effective transit time. The shorter the effective transit time, the wider the frequency bandwidth. Because of this characteristics in frequency response, the optical antenna made of regular MZI device will not exhibit dipole-like azimuthal omni directionality in the higher frequency range. However, if the light in the MZI arms can propagate in opposite direction with each other, then the accumulated phase change due to longer effective transit time in one arm will be compensated by that due to the shorter effective transit time no matter what propagating angle of RF is. As an example, the accumulated phase change for a parallel/counter-parallel case can be expressed as

$$\Gamma(t) = a_{EO} EL \frac{\sin(\frac{\omega\tau_{para}}{2})}{(\frac{\omega\tau_{para}}{2})} \sin[\omega(t - \frac{\tau_{para}}{2})] + a_{EO} EL \frac{\sin(\frac{\omega\tau_{count}}{2})}{(\frac{\omega\tau_{count}}{2})} \sin[\omega(t - \frac{\tau_{count}}{2})] \quad (12)$$

The frequency response of this parallel/counter-parallel case is also shown in Fig. 2 for comparison, where it resembles the perpendicular case up to 6.5 GHz, and level off after that. In the following section, we will report the fabrication and test of such an E-field sensor that exhibits omni directionality azimuthally. The test data indicates its frequency response behavior agrees fairly well with the theoretical prediction.

2.2 $LiNbO_3$ vs. EO Polymer

It is instructive to analyze the impact of MZI length, L, on the optical antenna performance. We modeled the expected RF signal picked up by using $LiNbO_3$ device versus EO polymer device using certain parameters.

Since the modulated light output of the E-field sensor can be expressed as in Eq. 1, where the input-output transmission T_{IO} is composed of both fiber coupling losses and the attenuation loss inside the MZI waveguides. In other words, T_{IO} can be expressed as

$$T_{IO} = k_c \exp(-\alpha L) \quad (13)$$

where k_c is the fiber coupling factor, α is the optical attenuation coefficient in the waveguide, and L is the MZI length.

Since the RF signal is proportional to the square of the modulated light output, from Eqs. (1), (2) and (13), the RF signal versus MZI length L can thus be expressed by

$$RF \propto L^2 \exp(-2\alpha L) \quad (14)$$

Figure 3 is a plot of $L^2 \exp(-2\alpha L)$ versus L at several α values. For a typical $LiNbO_3$ waveguide, the attenuation coefficient is 0.2 dB/cm. Therefore, a long $LiNbO_3$ device such as 10 cm will have better sensitivity. On the other hand, the cutting edge EO polymer developed by University of Washington (and EO polymer, in general) will have attenuation coefficient of about 1 to 1.5 dB/cm. The optimum device length will be only about 3 cm according to Fig. 3.

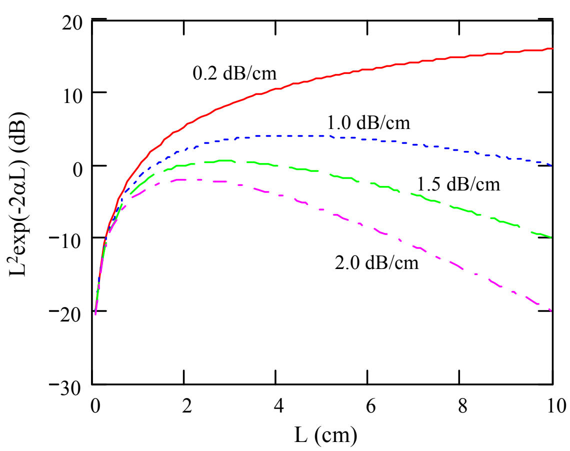

Fig.3. Expected RF signal versus the device length of MZI field sensors with various attenuation losses.

As for performance comparison between $LiNbO_3$ MZI device and EO polymer MZI device, we list in Table 1 some of the parameters we used in the simulation. Note that the values of r_{33} and α here for EO polymer are those we expect from UW such as AJL8 or AJLS102. By substituting these parameters into Eqs. (1) and (14), we plot the expected RF signals from $LiNbO_3$ and EO polymer devices in Fig. 4. As shown in the figure, an optical antenna using 5 cm $LiNbO_3$ device has much better performance than EO polymer device.

Table 1. Simulation parameters of $LiNbO_3$ and EO polymer MZI devices

	LNB	polymer	
λ	1.55	1.55	µm
n	2.2	1.6	
r_{33}	30	150	pm/V
$n^3 r_{33}$	319	614	pm/V
k_C	-1.5	-1.5	dB
α	-0.2	-1.5	dB/cm

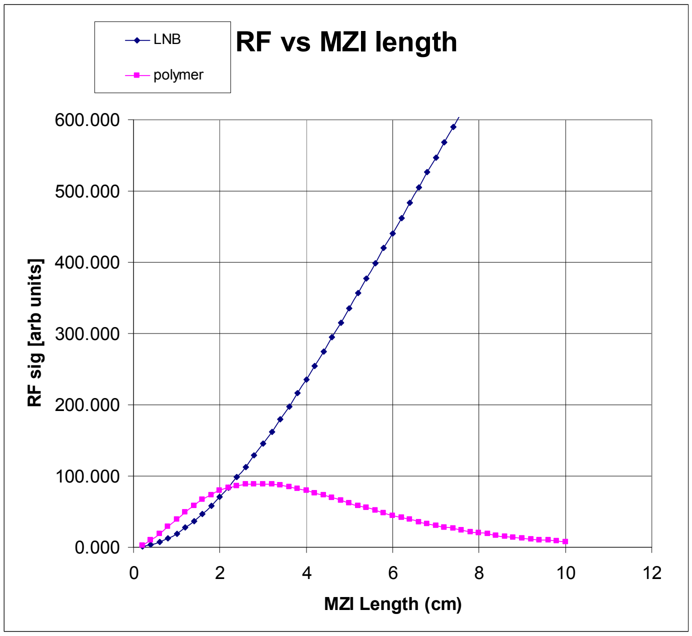

Fig.4. Performance comparison between $LiNbO_3$ and EO polymer devices with the parameters listed in Table 1.

3. $LiNbO_3$ E-FIELD SENSOR

3.1 Device Fabrication

A pair of 49 mm long z-cut $LiNbO_3$ (LNB) channel waveguide chips with PM fiber pigtailed was acquired from SWT. To make a MZI device with push-pull configuration, we attached these chips onto a glass substrate with one chip flipped over so its r_{33} direction is opposite to the other chip (see Fig. 5A). The whole assembly was installed inside an all-dielectric package before it was connectorized (see Fig. 5B). Its insertion loss from fiber to fiber is about 3 dB (T_{IO} ~ 50%).

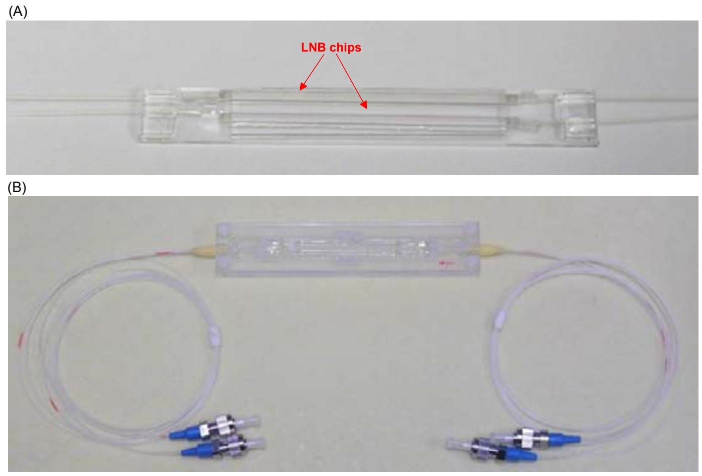

Fig.5. Picture of a push-pull LNB field sensor, where (A) was installed inside an all-dielectric package in (B).

To have MZI effect, a 30/70 PM coupler, a LNB phase modulator (for bias control purpose), and a 50/50 PM coupler were added to form a extended MZI. A schematic diagram of such a extended MZI design is shown in Fig. 6. Here a ditherless modulator bias controller (MBC, acquired from YY Lab) was used together with two tap couplers (95/5) for its two PD's. One of the 95/5 throughputs went to the transceiver (for RF output) and the other went to power meter for optical power monitoring. When the extended MZI is at the optimum quadrature point, the two complimentary outputs will have the same amplitude. Otherwise, there will be a difference, which is proportional to the offset of the working point from the quadrature point. Using two tap couplers to split a partial of the light from each output arms, the ditherless MBC continuously (sub-millisec response) detects the optical power difference and sends feedback to maintain optimal phase on phase modulator, and quadrature bias of the optical antenna. An important benefit of the ditherless MBC over typical MBCs is that it does not utilize pilot tones; therefore, it does not disturb the system. To have an E-field sensor exhibiting omni directionality azimuthally using parallel/counter-parallel configuration, the connectors A and B in Fig. 6 are switched so the light propagates in top arm is opposite to that in the bottom arm.

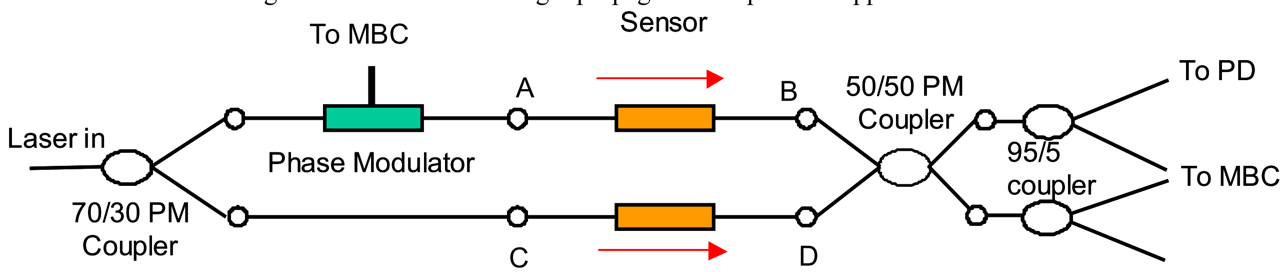

Fig. 6. A schematic diagram of an extended MZI field sensor device that includes a pair of LNB waveguides and a phase modulator.

3.2 Test of E-field Sensor

To test the E-field sensor, the LNB device of Fig. 5 was put inside a GTEM cell (acquired from ETS Lindgren, see Fig. 7), which can generate a fairly uniform E-field of about 10 V/m from kHz up to 5 GHz by a 20 dBm RF source. As can be seen in Fig.7, there are four bulkhead adaptors on the GTEM cell for the fiber connection between the LNB device inside and the outside components. Except LNB device, all the components shown in Fig. 6 and the power supply were put inside a metal container to prevent RF pickup by phase modulator, laser, and photo detector. To ensure the optimal signal sensitivity and stability, the bias of this extended MZI was controlled by a ditherless MBC at quadrature point. The RF signal carried by optical beam was converted back to electric signal by a wideband photo detector that was amplified by a low noise amplifier (LNA) and then analyzed by a RF spectrum analyzer.

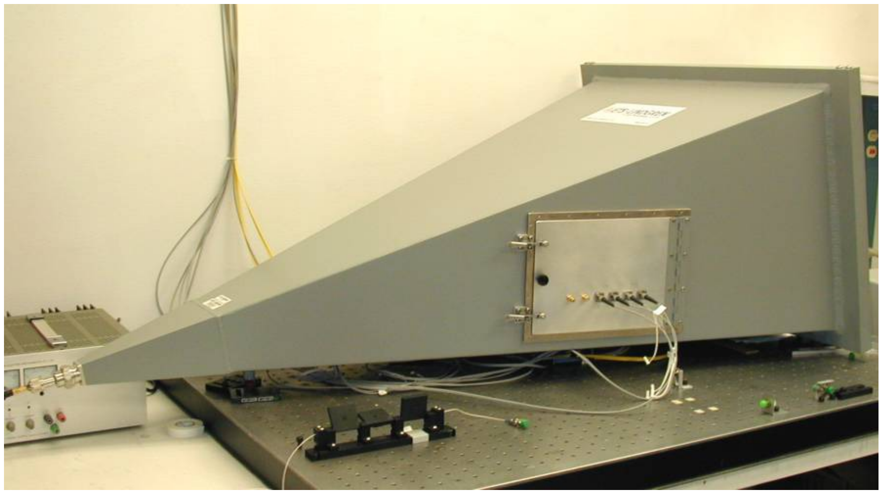

Fig. 7. A picture of a GTEM cell that can generate a fairly uniform E-field from few kHz to 5 GHz.

Inside the GTEM cell the LNB device was oriented such that its waveguides were parallel to the RF propagating direction. By switching the four fiber connectors outside the GTEM cell in certain ways, the RF wave could be parallel, counter-parallel, or parallel/counter-parallel to the optical beam without moving the LNB device.

A typical spectrum of detected RF at 60 MHz is shown in Fig. 8, where the RF, with an E-field strength of about 10 V/m, propagates parallel with optical beam. According to this data, the sensitivity of the field sensor can be determined and it is about 18 mV/mHz$^{1/2}$. The sensitivity can be further reduced by lowering the noise floor on the spectrum analyzer, which can be done by using better photo detecting system such as balanced photo detector for laser RIN noise reduction.

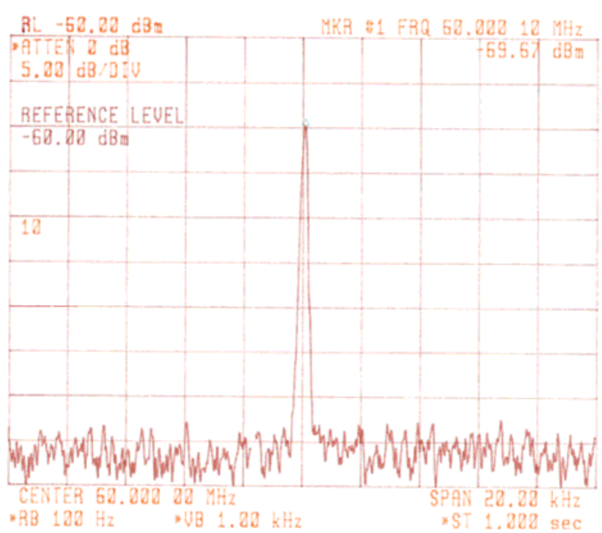

Fig. 8. A typical RF spectrum detected, where the RF frequency is at 60 MHz and its E-field strength is about 10 V/m.

In Fig. 9 we show the frequency response of this sensor from 30 MHz to 5 GHz with RF wave parallel, counter-parallel, and parallel/counter-parallel to the optical beams inside the LNB waveguides. The theoretical calculation of the expected frequency response (see Section 2.1) is also displayed by the continuous lines in Fig. 9 for comparison. The calculation is based on a 49 mm long EO section, with optical refraction index of 2.2. The refraction index associated with the propagating RF field is assumed to be 1 due to the very shallow penetration [in wavelength units] of the RF wave into the optical waveguide structure.

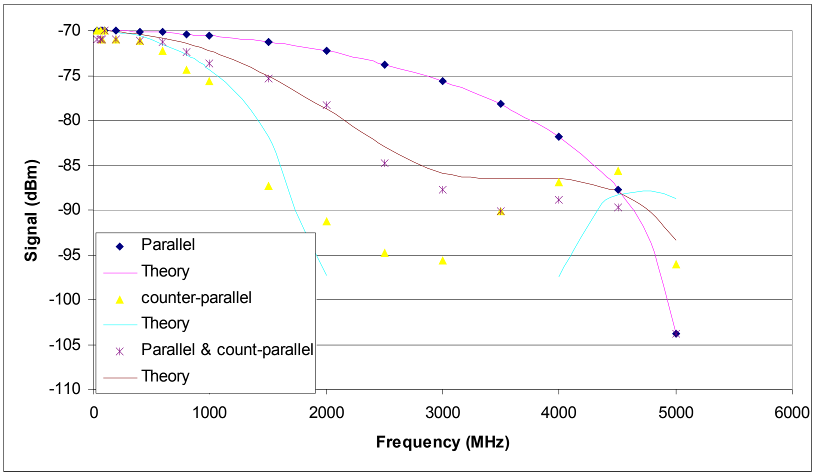

Fig. 9. Frequency response measurement of the LNB field sensor, where the RF wave propagation direction is parallel, parallel/counter-parallel, or counter-parallel with the light probe. The solid lines are the calculated response based on transit time considerations.

The parallel (optical and RF wave directions) configuration has the widest bandwidth; the counter-parallel configuration has the fastest roll off; and the parallel/counter-parallel configuration fits as expected in between. In the case of parallel/counter-parallel, we verified that the optical antenna sensitivity is independent on the RF direction azimuthally. In order to arrive at these comparisons, we needed a reliable sensor signal method to normalize the data sets. We noted from the GTEM operation manual that the E-field generated inside the cell is "fairly uniform" for frequency up to 5 GHz, but it still exhibits variations of more than 6 dB attributable to various factors that are difficult to control. A 6 dB variation in E-field strength translates into 12 dB variations in RF signal on plots in Fig. 9. Since there exists no other super wideband E-field sensor that can be used to calibrate the GTEM cell, we chose to normalize all data to the parallel-aligned case. Its frequency response follows the theoretical prediction fairly well.

3.3 Optical Transceiver with RF Output

To build an advanced optical antenna unit, which is compact, small size and weight, and low power consumption, we constructed a compact optical transceiver (see Fig. 10) for the all-dielectric E-field sensor. This transceiver includes a 1550 nm DFB laser, laser driver, MBC, PD, and LNA. This module has a size of 40 cubic inches, weights one pound, and consumes less than 10 watts of power. To accommodate the other components such as phase modulator and tap couplers to be used for extended MZI field sensor, a slightly bigger transceiver module will be constructed.

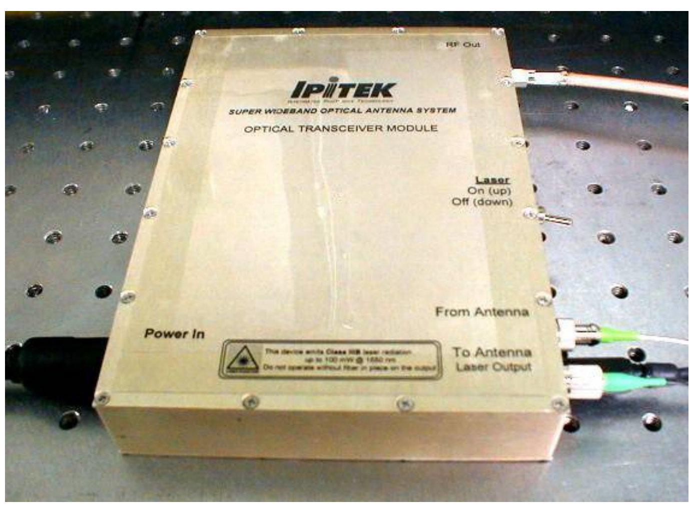

Fig. 10. A picture of the newly finished optical antenna transceiver modules.

CONCLUSION

An all-dielectric LNB extended MZI device was demonstrated with sensitivity to free-space E-field RF signals over a wide frequency range from 30 MHz to 5 GHz. The frequency response of the LNB device agrees well with modeling prediction. A novel configuration of extended MZI device with optical beams propagate opposite with each other exhibits dipole-like azimuthal omni directionality. With the extended MZI design, a bias-stabilized all-dielectric field sensor is possible. This sensor has detection limit of about 18 mV/(m√Hz), which can be further improved by using better photo detecting system.

ACKNOWLEDGEMENT

This work was supported by US Army CECOM under contract W15P7T-07-C-P008.

---

[1] W.C. Wang, H. Lotem, D.Y. Zang, R. Forber, Stephen Schultz, and Richard Selfridge, "Dielectric Ultra Wideband Optical E-field Sensors", *SPIE,* vol. 6219, p.62190F, (2006).

[2] W.C. Wang, H. Lotem, R. Forber, and K. Bui, "Optical Electric-field sensors", *Optical Engineering*, **45**(12), p.124402, (2006).

[3] R. Forber, W.C. Wang, D.Y. Zang, S. Schultz, and R. Selfridge, "Dielectric EM Field Probes for HPM Test & Evaluation," Annual ITEA Technology Review, Cambridge, MA (2006).

[4] J. Berger, K. Petermann, H. Fahling, and P. Wust, "Calibrated electro-optic E-field sensors for hyperthermia applications," Phys. Med. Biol., **46**, 399-411, (2001).

[5] Y. Enami, C. T. Derose, D. Mathine, C. Loychik, C. Greenlee, R. A. Norwood, T. D. Kim, J. Luo, Y. Tian, A. K.-Y. Jen and N. Peyghambarian, "Hybrid polymer/sol–gel waveguide modulators with exceptionally large electro–optic coefficients," Nature Photonics Vol 1, pp 180-185, (2007).

[6] Z. Shi, S. Hau, J. Luo, T.D. Kim, N.M. Tucker, J.W. Ka, H. Sun, A. Pyajt, L. Dalton, A. Chen, and A.K.Y. Jen, "Highly Efficient Diels–Alder Crosslinkable Electro-Optic Dendrimers for Electric-Field Sensors," Adv. Funct. Mater. **0000**,00, 1-8, Wiley-VCH (2007).

[7] D. Chen, H.R.Fetterman, A. Chen, W.H. Steir, L.R. Dalton, W. Wang, and Y. Shi, "Demonstration of 110 GHz electro-optic polymer modulators", *Appl. Phys. Lett*. 70(25), 3335-3337 (1997).

[8] Amnon Yariv, "*Quantum Electronics*", John Wiley & Sons Chap. 14 (1975).